*Pure Appl. Chem.*, Vol. 74, No. 9, pp. 1593–1607, 2002.


# Structure and dynamics of monolayers on planar and cluster surfaces*

T. Pradeep‡ and N. Sandhyarani§

*Department of Chemistry and Regional Sophisticated Instrumentation Centre, Indian Institute of Technology Madras, Chennai 600 036, India*

*Abstract*: Organized molecular assemblies have been one of the intensely pursued areas of contemporary chemistry. Among the various methodologies used to make organized monolayer structures, self-assembled monolayers (SAMs) have been attractive to many materials chemists owing to the simplicity of the preparative method and high stability. Advances in various techniques and their application in the study of SAMs have significantly improved our understanding of these molecular systems. These studies have been further intensified since the successful preparation of stable metal clusters protected with monolayers. This article reviews the structure, temperature-induced phase transitions, and associated dynamics of monolayers, principally in the context of our own work in this area. Alkanethiols on Au(111) and Ag(111) are taken as archetypal systems to discuss the properties of 2D SAMs; studies from our laboratory have been on evaporated thin films. Alkanethiols on Au and Ag cluster surfaces are taken as examples of 3D SAMs. Although our principal focus will be on alkanethiols, we will touch upon a few other adsorbate systems as well.

## INTRODUCTION

An important aspect of modern technology is the role of surfaces and interfaces. Of the several processes occurring at surfaces, adsorption has been widely appreciated and intensely explored [1]. Formation of ultrathin films at interfaces [2] has been recognized for well over a century, which determines fundamental properties such as friction, lubrication, etc. Spontaneous growth of monolayers was suggested by Zisman and coworkers in 1946 [3]. They observed that alkyl amines adsorb on platinum, and spontaneous formation of an ordered monolayer occurs. The molecular films formed are known as self-assembled monolayers (SAMs). SAMs are defined as ordered molecular assemblies formed by the adsorption of an active surfactant on a solid surface. During the early period, the potential of SAMs was not recognized. In 1983, Nuzzo and Allara showed that SAMs of alkanethiolate on gold could be prepared by the adsorption of *n*-alkyl disulfides from dilute solutions [4]. Following this report, a rapid growth in SAMs research occurred. Several adsorbate/adsorbent combinations have been found [5,6]. Among these, alkanethiol monolayers on coinage metals, especially gold, became the center of attraction because of its inertness (so that a clean absorbent can be made even in normal laboratory conditions) and owing to the fact that the formed monolayer is stable as Au–S bond is sufficiently strong [7] (bond energy ~48 kcal/mol). The ability to tailor the monolayer–air interface makes SAMs ideal model systems for studies of interfacial phenomena. Potential applications of these systems include sensors [8], corrosion inhibitors [9], molecular recognition [10], and molecular crystal growth [11]. Real applications of these systems require precise control of structural features [12]. The number of molecules on

**Pure Appl. Chem.* **74**, 1489–1783 (2002). An issue of reviews and research papers based on lectures presented at the 2nd IUPAC Workshop on Advanced Materials (WAM II), Bangalore, India, 13–16 February 2002, on the theme of nanostructured advanced materials.
‡Corresponding author: Fax: ++91-44-257 0509/0545; E-mail: pradeep@iitm.ac.in
§Currently at Cornell University, USA

a planar surface is less (~$10^{15}$ molecules per sq. cm of the surface), which makes it difficult to use conventional characterization techniques for their study. Therefore, it is necessary to increase the number of assembled molecules within the area of investigation, which is possible if the molecules are assembled on the surface of a nanocluster.

In 1994, Brust et al. reported the synthesis of monolayer-protected metal clusters (MPCs) in a two-phase synthesis method [13]. It has been identified that about 60 % of the metal cluster surface is covered, whereas the coverage is only 30 % on planar or 2D surfaces. MPCs are important in technology not only by giving a higher number density of molecules at the surface but also by preserving the nanodimension of the cluster. Being a soluble powdery nanomaterial, these clusters allow conventional techniques for their characterization, owing to larger quantities of the monolayer surfactant as a consequence of the high surface area (ca. 100 $m^2/g$).

Apart from the fundamental understanding of their structure, phase transition of monolayers as a function of temperature is important from other angles. Importance of the structure and phase of SAMs in the surfactant, wetting, etc. properties show the need to understand the phenomena in detail. Application of monolayer systems require a precise knowledge of the phase behavior and structural transformations. Temperature dependence of the molecular organization and structure is important while considering realistic applications.

There have been several reviews of various aspects of SAMs [14–18]. An interested reader may consult them for a historical introduction and a more detailed consideration of any of the specific aspects of the subject. In the following, we shall first give a concise introduction to self-assembled monolayers on planar and cluster surfaces so that the specifics provided later can be appreciated. The objective will not be to review the literature, but to present the most significant aspects of monolayer research, within the context of our work in this area. We are aware that owing to the limited scope of this review as well as the space restrictions, several important works are not cited and even those cited are not adequately discussed.

## ADSORPTION AND STRUCTURE OF SAMs

It has been well established that alkanethiols form well-ordered monolayers on Au(111) and Ag(111) surfaces. Extensive X-ray photoelectron spectroscopic (XPS) experiments suggest that chemisorption of alkanethiols on gold (0) surface yields the gold (I) thiolate ($R–S^-$) species, while the mechanism is not clear completely. The presumed adsorption chemistry is,

$$R\text{-}SH + Au_n^0 \rightarrow RS^- - Au^+ + 1/2\ H_2 + Au_{n-1}^0$$

Absence of S–H stretching in the IR spectrum suggests the loss of hydrogen from thiol. This loss may happen either via the reductive elimination reaction of the gold (II) hydride (which is formed by the oxidative addition of the alkanethiol) or by the elimination of hydrogen as shown above or as water in presence of an oxidant. However, using electrochemical measurements, Paik and colleagues showed that it is not a simple mechanism, and an electrochemical oxidation route is involved [19,20]. The formation of alkanethiol SAMs is suggested to involve an anodic reaction, $RSH + Au \rightarrow RS–Au + H^+ + e^-$.

Recently, we have found that hydrogen is evolved during thiol adsorption [21]. To study this, mass spectra were recorded as a gold film surface was exposed to thiol. By careful monitoring of the various gas-phase species, we concluded that the initial pinning of thiol involves hydrogen evolution. Experiments were performed with several thiols using gold and silver surfaces.

Even though the mechanism of SAM formation is still in debate, the structure of the monolayer is almost clearly understood. Electron diffraction and STM measurements reveal that the monolayer forms a $(\sqrt{3} \times \sqrt{3})$ R30° overlayer structure on Au(111). Zarinkov et al. demonstrated that hybridization and, thus, the spatial orientation of the bonding orbitals of sulfur is the determining factor for the orientation and density of the alkanethiol monolayer rather than the intramolecular interaction [22]. The

surface order can extend over hundreds of square nanometers, and the symmetry of the sulfur atoms is hexagonal. The sulfur–sulfur interactions are believed to be minimal. This distance is greater than the distance of closest approach of the alkyl chains (4.24 Å), which makes the monolayer undergo a tilt. This tilt angle ($\alpha$) is found to be 30° with respect to the surface normal toward the nearest neighbor direction. Fenter et al. demonstrated a systematic dependence of the tilt structure (tilt angle and direction) with the chain length, which is explained as due to the change in intralayer interaction strength [23]. The twist angle $\beta$ (which defines the rotation of the carbon chain backbone about the chain axis with respect to the plane defined by the chain axis and the surface normal) for the long-chain alkanethiol is found to be ~52°, which implies that Au–S–C bond angle is nearly 120°, close to the optimum value for the $sp^2$ hybridized sulfur atoms. Scanning tunneling microscopy (STM) measurements reveal the existence of hexagonal patterns as well as several variants of $c(4 \times 2)$ superlattices [24]. This study further showed that the domain boundaries are oriented along the next-nearest-neighbor directions of the sulfur lattice. Various studies suggest that the polymethylene chains are fully extended, tilted with respect to the surface normal, and are in nearly all-trans configuration. With increasing chain length of the adsorbed thiol, the thickness increases linearly. For smaller chain length, a liquid-like behavior is observed at room temperature. It has been shown that vacancy islands (holes) are being generated during the self-assembly process [25], and this can be healed out by thermal annealing at 350 K [26].

Alkanethiols on Ag(111) form a $(\sqrt{7} \times \sqrt{7})$ R10.9° structure with an S–S distance of 4.41 Å. Because of this shorter S–S distance, alkanethiols on Ag are more densely packed. There are varying reports, however, the orientation is proved to be almost perpendicular to the surface on clean Ag(111) surfaces [27]. It has been shown that the $(\sqrt{7} \times \sqrt{7})$ R10.9° structure observed in the short-chain alkanethiols cannot be extended to the long-chain alkanethiolates because of the larger interchain van der Waals interaction. Suggested mechanism for the formation of alkanethiolate SAMs on Ag(111) surface is the initial formation of $(\sqrt{7} \times \sqrt{7})$ R10.9° structure and its distortion upon saturation coverage owing to the increase in van der Waals interaction. In a recent article, Zharnikov and Grunze looked at the similarities and differences in the behavior of alkanethiols on Au and Ag surfaces [28]. They demonstrated that the decisive factor for the structure and bonding in these systems is the head-group substrate interaction.

Although the literature is full of detailed investigations of alkanethiols, only very limited information exists on arenethiols. 1,4-Benzenedimethanethiol ($HS–CH_2–C_6H_4–CH_2–SH$, BDMT) adsorbs dissociatively on planar silver and gold surfaces yielding self-assembled monolayers with the thiolate structure [29]. Whereas the molecule adsorbs flat on Ag as a result of the loss of two thiol protons, the molecule stands vertically on Au, losing only one thiol proton. BDMT monolayers are more stable than alkanethiol monolayers and desorb only at a fairly high temperature of 423 K in air, whereas alkanethiols desorb below 373 K. An increase in temperature leads to structural changes in the Au monolayer, and the molecules begin to lie flat on the surface, and desorption occurs from this state. The Ag monolayer is less stable thermally and desorption is eventless. The evolution in the structure of the monolayer as a function of adsorbate concentration was studied by Kim et al. [30].

The presence of thiol proton makes it possible to attach organic and inorganic moieties at the monolayer surface. Exposure of metal ions ($Cu^{2+}$, $Ni^{2+}$, and $Zn^{2+}$) to 1,4-benzenedimethane thiol monolayers on Au results in the formation of metal-functionalized monolayers [31]. The thiol group ($\nu_{SH} = 2563\ cm^{-1}$) at the surface is not detectable after exposure, indicating that the metal ions replace the protons of the thiol group (Fig. 1). Metal ion reaction leads to a red shift in the C–S stretching frequency, and most of the other features are unaffected. Relative intensities of the peaks are largely unaffected; however, some new features are observed, suggesting minor changes in the adsorbate structure, which makes other frequencies observable. Thermal stability of the monolayers has been reduced substantially as a result of reaction with metal ions, indicating that the electronic structure of the Au-monolayer interface is affected by the metal ions. Electrochemical behavior before and after metal ion adsorption is significantly different, and the adsorbed metal ions undergo reversible redox transformations. Reactions of monolayers can also be effected in solution as shown in the case of 2-mercaptobenzothiazole (MBT) monolayers [32].

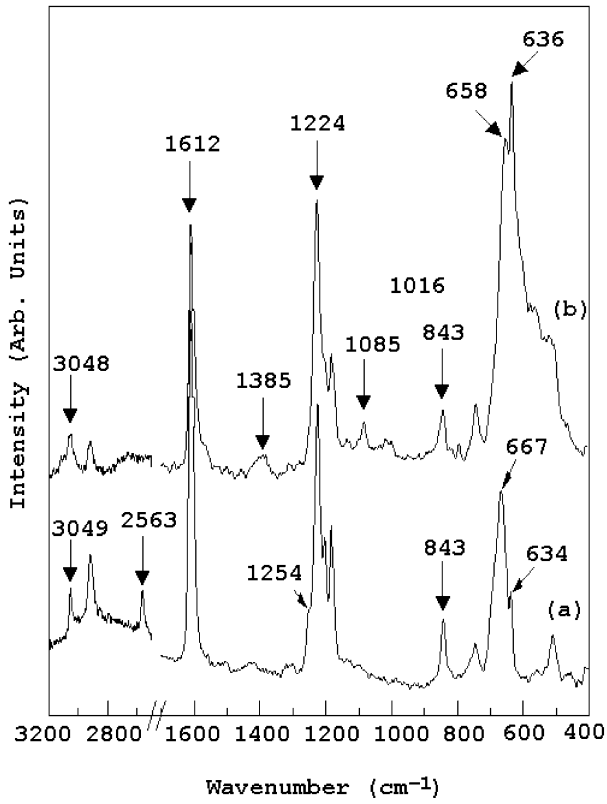


**Fig. 1** Surface-enhanced Raman spectra of (a) bare BDMT monolayer on Au and (b) the monolayer exposed to $Cu^{2+}$ ions. The peaks of significance are marked. Note that the S–H stretching mode at 2563 $cm^{-1}$ in the free monolayer is absent in (b). Other important frequencies are marked. Certain new features emerging in (b) which are also indicated. See the original reference for a detailed discussion (from Venkataramanan et al. [31], copyright American Chemical Society).

Although sulfur ligands have been investigated extensively, very little has been done with the corresponding selenium systems [33]. SAMs of dialkyl chalcogenides on Au(111) have been studied by Nakamura et al., and they found that selenides form ordered monolayers on Au(111) with long exposure time, whereas tellurides form disordered monolayers [34]. A detailed investigation of the self-assembled monolayers of diphenyl disulfide (DDS), diphenyl diselenide (DDSe), and naphthalene disulfide (NDS) on polycrystalline gold films was performed recently [35]. Whereas DDS dissociatively chemisorbs on Au, in both DDSe and NDS, the Se–Se and S–S bonds, respectively, are preserved upon adsorption. All of the molecules adsorb with the molecular plane perpendicular to the surface.

In cases where there is an equilibrium between two different forms of the adsorbate, whether the surface shows preference for any form is an important question. The monolayers of 2-mercaptobenzothiazole (MBT) on polycrystalline Au and Ag films have been studied to understand this [37]. Whereas MBT adsorbs with its molecular plane flat on Ag, it is perpendicular on Au. Adsorption geometry is manifested as differences in the intensities of certain peaks in the Raman spectra. Ab initio molecular orbital (MO) calculations suggest that MBT adsorbs on Au in the thione form and on Ag in the thiol form.

While spectroscopies of various forms have been useful in understanding diverse aspects of monolayer chemistry, definitive information on their structure can also be derived from other techniques. Reactive scattering of low-energy ions from surfaces gives scattered product ions in which new

bonds are formed with the adsorbate with sensitivity to the adsorbate geometry. Reactions of $Cr^{\bullet+}$ and $C_5H_5N^{\bullet+}$, as well as chemical sputtering induced by $Xe^{\bullet+}$, are used to distinguish two monolayers, namely 1,4-benzenedimethanethiol adsorbed on Au(111) and Ag(111) films [38]. While the reaction of $Cr^{\bullet+}$ with the Au monolayer produces an ion assigned as $CrC_7H_5S^+$, this product is completely absent upon reaction with the Ag monolayer. Pyridine ($C_5H_5N^{\bullet+}$) projectiles abstract $C_1$–$C_8$ hydrocarbon groups in 50 eV collisions with the Au monolayer, while the Ag monolayer shows only $C_1$–$C_4$ abstraction with a significantly different intensity pattern. Chemical sputtering ($Xe^{\bullet+}$) mass spectra of the two surfaces are substantially different; complete fragmentation of the Ag adsorbate occurs, leading to $C_2$–$C_4$ ion ejection, while more of the molecular features are preserved in the spectrum recorded for the Au monolayer. The experimental facts are explained in terms of the difference in the adsorption geometry of the BDMT molecule. A similar study has been done to differentiate isomeric chemisorbates [39]. Reactions of $Cr^{\bullet+}$ and Cr-containing cations at chlorobenzyl mercaptan (CBM) monolayers on Au surfaces show different reaction products, depending on the position of chlorine substitution in the phenyl ring.

## PHASE TRANSITIONS

Conformational transitions play a major role in the temperature-dependent phase behavior and dynamics of molecular thin films. Importance of different phases in the surfactancy, wetting, etc. properties shows a need to understand the microscopic details of such phenomena. Only a limited number of studies have addressed the issue of phase transitions of alkanethiol monolayers on Au surfaces. Recent investigations have shown that heating induces changes in the vibrational, conformational, and positional order parameters. These studies show that vibrational spectroscopic measurements are sensitive to the conformational order, and, on the other hand, diffraction and scanning probe measurements are sensitive to the spatial position of the molecule.

Evolution in the equilibrium structure of monolayers has been an important aspect of research. An extensive surface-enhanced Raman spectroscopy (SERS) investigation of alkanethiol monolayers on Au and Ag surfaces has been carried out by Bryant and Pemberton [40,41]. SAMs of $CH_3$ $(CH_2)_n$ SH ($n$ = 2, 5, 7, 8, 9, 11, and 17) on polycrystalline gold films also have been investigated using FT-Raman spectroscopy [42]. All the thiols chemisorb dissociatively in the thiolate form, and the adsorbate-surface interaction is the same in all the cases. Initial chemisorption occurs with fast kinetics, and it is complete in the first few hours of exposure of the thiol to the surface. The formation of self-assembly occurs rather slowly, and the evolution of spectral features continues until 12–15 h of exposure. The change is pronounced particularly on the $(C–C)_T$ stretching mode. Initial adsorption results in the $(C–S)_G$ form, and equilibration between $(C–S)_T$ and $(C–S)_G$ occurs rather quickly. In lower-member thiols, equilibration occurs within about 30 min of exposure. A temperature-dependent study was undertaken to understand the thermal stability of monolayers (Fig. 2). The $(C–C)_T$ is reduced in intensity upon increasing the temperature, and the spectrum at 348 K can be compared with that of the liquid, suggesting melting of the monolayer. Monolayer desorption is observed beyond this temperature.

Alkanethiol self-assembled monolayers of varying chain lengths have been studied by X-ray photoelectron spectroscopy [43]. Inelastic background of the S2p peak monotonically increases with the chain length. The binding energies and peak shapes are the same for all the samples studied, indicating the chemical similarity of the monolayers. However, increased packing density is seen with hexane and octanethiol SAMs, suggesting greater surface order. It is proposed that in higher and lower thiols, random orientation of the chains decreases packing density. Inelastic background of the S2p peak is directly proportional to the ellipsometric thickness of the monolayers.

During the low-energy helium diffraction experiments on alkyl thiol monolayers on gold, Chidsey et al. [44] found that the diffraction peaks gradually lose intensity as the surface temperature is raised, and the peaks disappeared around 100 K. Disappearance of the specular peak is observed at 300 K.

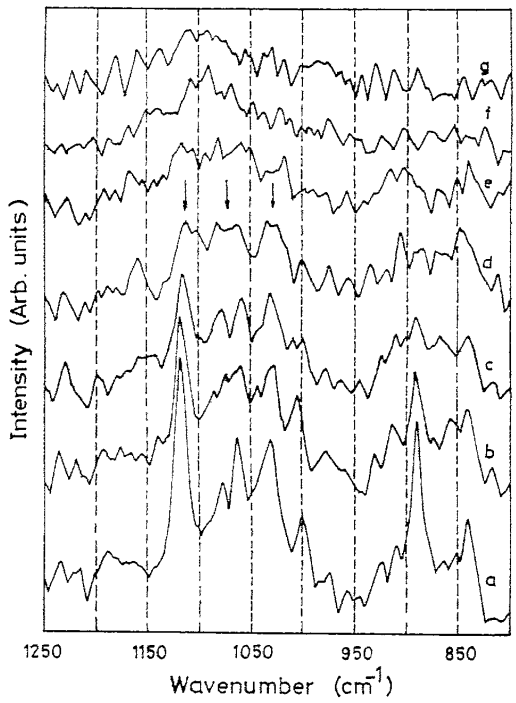


**Fig. 2** SER spectra of the C–C stretching region of octane thiol monolayer as a function of temperature. (a) 301 K, (b) 323 K, (c) 348 K, (d) 373 K, (e) 398 K, (f) 423 K, and (g) 448 K. Principal effect seen upon heating is the reduction in the intensity of the $(C–C)_T$ mode at 1122 $cm^{-1}$. Arrows indicate the emergence of "liquid-like" structure above 348 K (adapted from Sandhyarani and Pradeep [42], copyright Elsevier Science).

They attributed this result to the thermal motion of the $CH_3$ group located at the surface. This has been further confirmed by Camillone et al. [45], who suggested an increase in thermal motion with increase in temperature. This finding is consistent with the experiment by Nuzzo et al. [46], who used IR spectroscopy to show that the alkyl chains undergo a phase transition, below 300 K from an ordered phase to another ordered phase, and the transition temperature is chain length-dependent.

Molecular dynamics (MD) simulations suggest a sudden increase in rotational disorder at 200 K along with the onset of conformational disorder as temperature increases [47]. Direct experimental evidence for such a transition is still lacking, however, the IR data show a two sublattice low-temperature structure below 220 K. This simulation suggests a correlation between the rotator phase transition and the appearance of the conformations arising indirectly via the softening of torsional potential and enhanced flexibility of the chain backbone. As the temperature increases, a second transition occurs, the unlocking of the direction of tilting between 250 and 300 K. The tilt angle of the chains continues to decrease in temperature until above $T \sim 450$ K, the system no longer has a collective tilt. At this temperature, the molecules are freely rotating and have a high density of conformational disorder, which is distributed uniformly throughout the chain. Molecular dynamics study by Mar and Klein [48] using an all-atoms model reestablished the rotator phase and a high-temperature phase transition. This study shows a herringbone structure (two chains per unit cell) at low temperature, which is contradictory to the experimental observation of four chains per unit cell structure. Hautman and Klein suggested large amplitude librations and rotational jumps about the molecular axis at 300 K, rather than free rotation [49], using their MD simulations. Using Monte Carlo technique, Taut et al. [50] showed the 2D melting and a solid-phase transition. Both the low-temperature order–disorder transformation have been

observed in an MD simulation by Bhatia and Garrison [51]. Using Morse and Linnard–Jonnes potentials, Sadreev and Sukhinin calculated the P-T diagram of the SAMs. They claimed that three phase transitions are present in SAMs and all of them are first order [52].

The nature of alkyl-chain phase transitions has been investigated using infrared spectroscopy. In IR spectroscopy, the degree of disorder is measured on the basis of methylene stretching mode, and this is the most sensitive measurement of the conformational disorder. IR investigations suggest that gauche conformations are concentrated at the chain termini, which decrease with decreasing surface temperature [53]. Comparing the influence of temperature on the methyl and methylene modes, Dubois et al. [53] showed the gauche defects are concentrated at the chain termini and as the temperature is raised, the methyl surface melts first and progresses toward the surface methylenes. Nuzzo et al. [46] observed that the monolayers are more ordered at 80 K. Conformation of the molecules is more all trans, and two alkyl chains per unit cell are observed. In these experiments, a peak assigned to the methylene group asymmetric scissoring motion is observed to split into two as the temperature is lowered from room temperature. However, IR evidence for the orientational phase transition has not been observed in low-temperature diffraction experiments.

Reflection absorption infrared spectroscopy (RAIRS) investigations at near grazing incidence show a phase transition from crystalline state to a liquid-like state at around 350 K [54]. The upward shift of peak frequency and decrease in peak height as well as increase in peak width are indications of this phase transition. This solid–liquid phase transition is gradual and irreversible unlike in lipid bilayers.

A two-step phase transition has been observed in RAIRS experiment on a series of alkanethiol SAMs [55]. A reversible structural change, which is a result of the untilting of the alkyl chain, is observed around 320 K, whereas a complete irreversible transition is observed above 350 K. This irreversible transition is due to the increase in the conformational disorder throughout the chain. Variation of the $CH_2$ symmetric stretching intensity with temperature follows the variation of the polar tilt angle. This confirms the high sensitivity of IR to changes in the tilt angle. This variation is in accordance with the MD simulation for a $C_{13}$ thiolate SAM, which suggests that the chains gradually untilt as the temperature is raised from 40 to 375 K, with the average tilt angle varying from 35° to 24° to the surface normal. The increase in intensity after 350 K is attributed to the formation of conformational disorder in the chains, leading to a random orientation of the methylene groups, which is perpendicular to the surface. In addition to the integrated intensity, the upward shift of the frequency also resulted from the increase in conformational disorder.

Phase-transition studies of alkanethiols on Ag surfaces are relatively less. Bensebaa et al. used silver alkanethiolate layered materials for phase-transition studies [56]. They have shown that alkanethiols undergo a melting transition at higher temperature, as in the case of Au SAMs. We have shown that layered octadecanethiolate melts at 400 K, much higher than the phase-transition temperature of planar monolayers [57]. This is attributed to the increase in van der Waals interaction as a result of the interdigitation of alkyl chains from the neighboring layer. Voicu et al. used specifically deuterated silver octadecanethiolate layered material and studied their phase-transition behavior using differential scanning calorimetry (DSC), variable-temperature IR, and variable-temperature NMR spectroscopies [58]. They too found a melting transition at 403 K, which was manifested as an increase in gauche population. Their study shows that the $C_1$ atom experiences a more restricted motion.

MD simulations as well as IR studies confirm two-phase transitions in the monolayers. The second phase transition has been proved by various experimental techniques. Fenter and coworkers performed a grazing-incidence X-ray diffraction study as a function of both chain length and temperature [59]. They showed different phases on the basis of tilt direction and constructed a ($n$,$T$) phase diagram. The phase transitions are dependent on chain length as well as temperature. As the temperature was increased to 343 K, a melting transition is observed in long-chain thiols with the coexistence of both solid and liquid phases at temperatures in the range 323–343 K. This transition involves a change in the thiolate packing from a hexagonal two-dimensional structure that is commensurate with the Au(111) substrate, to one that is incommensurate. The electrochemical studies by Badia et al. confirm the

order–disorder transitions in SAMs [60]. They too found a chain-length dependence of melting temperature, which varies between 313 and 338 K.

STM investigations suggest thermal motion of the alkanethiol monolayer at around 350 K, which in turn causes mobility for the topmost layer of the gold surface [61]. This mobility results in bigger holes or vacancy islands with triangular equilibrium shape. Upon extensive annealing at 350 K, the vacancy islands are annihilated at pre-existing substrate steps, leaving flat defect-free SAMs. The slow evaporation rate compared to the lateral mobility of the molecule allows the film to adopt new stable structures for each reduced coverage. This is in agreement with the increase in intensity of the peaks in IR investigations [55]. Recently, the phase transition in monolayers has been observed in an in-plane resistance measurement of the substrate [62]. Here, the observed increase in the slope of the resistance vs. temperature plot is attributed to the phase transition.

Poirier et al. proposed a two-dimensional phase diagram using variable-temperature ultrahigh vacuum (UHV) STM [63]. They determined the phase stability of the decanethiol monolayer as a function of temperature and showed that at a temperature of 300 K, three phases, namely, $\delta$, $\varepsilon$, and $\phi$, coexist, and at a still higher temperature of 306 K, $\chi$, $\delta$, and $\varepsilon$ phases are present, and these phases changes to $\chi$, $\varepsilon$, and $\beta$ at 308 K, and finally, at 328 K, $\varepsilon$, $\beta$, and $\alpha$ phases are manifested.

## MONOLAYERS ON CLUSTER SURFACES (3D SAMs)

As we have seen in the last sections, studies of monolayers on planar surfaces require more specialized techniques. Synthesis of monolayer-protected metal clusters (MPCs) help in the study of monolayers with conventional techniques. Nanoparticles synthesized by colloidal chemistry will tend to form non-equilibrium aggregates due to their strong interparticle interactions [64]. In order to prevent agglomeration, these nanostructured clusters usually need to be passivated with covalently bound ligands, for which various methods exist [13,65]. Thiol-passivated nanocrystals are found to be thermodynamically stable. These monolayers are commonly known as 3D SAMs to distinguish them from the conventional 2D SAMs. Alkanethiols give uniform protection to the cluster surface without modification of its essential structural and electronic properties. They form compact ordered monolayers in which thiolates attach to various cluster planes, and their spontaneous assembly is driven by the favorable van der Waals interactions.

MD simulations show that the equilibrium adsorption geometries of the monolayer depend on the alkyl chain length [66]. At low temperature, the molecules are bundled into groups with a preferential parallel intermolecular orientation of the molecular backbones in each bundle, and the bundles in turn are oriented with respect to each other. They showed that small clusters assume an irregular truncated octahedron morphology, and sulfur atoms bind to the middle hollow site of the small (100) facets, and on the (111) facets they arrange in a distorted hexagonal pattern with the atoms located in the middle as well as off the hollow sites, as shown in Fig. 3. The sulfur atoms are arranged in two alternating inequivalent geometries on adjoining (111) facets with S–S distances of 3.9 Å and 4.5 Å. In larger clusters, the sulfur atoms are arranged in a hexagonal pattern on (111) facets, with the center atom on the on-top site, and on the (100) facets they form a rhombus with the atoms adsorbed off the hollow sites. The S–S distances in these clusters are 4.1 Å (on the (100) facets) and 4.3 Å [on the (111) facets]. The nearest neighbor distance between Au atoms is ~2.8 Å. These distances suggest around 12 % contraction of the mean nearest neighbor distance between adsorbed sulfur atoms on planar Au(111) surfaces, which results in ~30 % increase in their packing density.

Structure of alkanethiolate monolayers in MPC solids has been probed in detail by $^{13}$C NMR [67] and transmission IR [68] spectroscopies. $^{13}$C NMR focuses on the dependence of chemical shifts as a function of the carbon position relative to the gold–hydrocarbon interface. The important findings here are, compared to the $C_8$ monomer and cluster, all the peaks are broadened in the cluster, which is attributed to the immobilization of the surfactant on the cluster surface. Going from shorter to longer chain lengths, the peak width narrows, as the carbon is located farther from the thiol functionality. Another

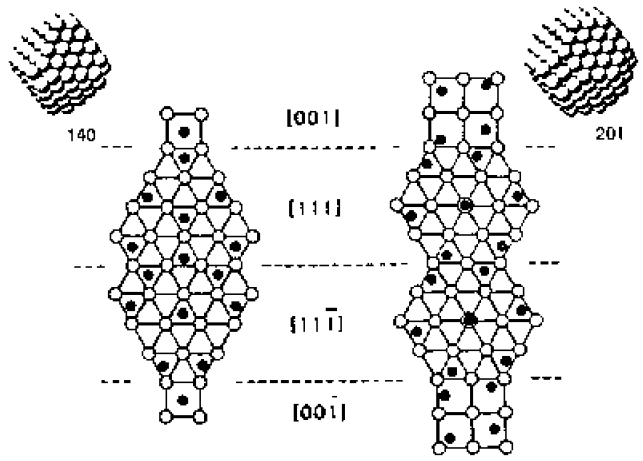


**Fig. 3** Arrangement of the sulfurs on the facets of gold cluster. Two clusters containing 140 and 201 atoms of gold are shown. The surfaces of these two clusters are spread showing the location of the sulfurs. Au atoms are open circles, and S atoms are filled circles (from Luedtke and Landman [66], copyright American Chemical Society).

significant observation is that the resonances from carbons closest to the Au core, those due to $C_\alpha$, $C_\beta$, and $C_\gamma$, are broadened into the baseline, and there is a systematic change in both the chemical shift and line width with the carbon position relative to the Au–hydrocarbon interface. These are attributed to the discontinuity in the diamagnetic susceptibility at the Au–hydrocarbon interface and residual dipolar interactions in alkanethiolate monolayers. Badia et al. compared the adsorption of thiols on a cluster surface with Au(1) alkyl thiolates and found that the chemisorbed species on the gold nanoparticle surface is a thiolate, not a disulfide [69]. They observed a line broadening of the $C_1$ and $C_2$ sites, which is explained as due to the chemical shift distribution resulting from the different adsorption sites and/or nonspherical particle shapes. These observations show the similarity of these 3D SAMs to the corresponding 2D SAMs. NMR data suggest that the long alkyl chain surfactant on gold nanoclusters is in a semicrystalline state. At room temperature, all-trans chains coexist with a smaller population of more mobile chains containing gauche conformers [67]. The shorter-chain thiols are disordered even at room temperature. Broadening of the resonances, as well as the disappearance of the carbons closest to the surface, show the immobilization of the alkyl chains and the strong interaction to the metal surface, respectively. The upfield shift of $C_{17}$ in $C_{18}S$–Au and the Gaussian decay of the signal in the dipolar dephasing experiments suggest the presence of a motionally restricted interior of the alkyl chain and conformationally disordered chain ends. The methyl proton line widths are lower than that of crystalline alkanes, which suggests that large amplitude motions are taking place about the chain axis.

We have studied the alkanethiols on silver clusters by IR spectroscopy [70]. Presence of $d^+$ and $d^-$ modes at 2850 and 2920 $cm^{-1}$ in the case of long-chain alkanethiols ($n$ = 8) shows the crystalline-like environment. Short-chain alkanethiols shows liquid-like behavior. Absence of S–H stretching indicates the loss of thiolate proton upon adsorption. It has been shown that a repeated heating-cooling cycle (up to a temperature of 200 degrees) results in the annealing of the monolayer on the surface [57].

We measured the mass spectra of the desorbed alkanethiols from the Au and Ag clusters [70]. In all the cases we saw, the peaks are due to $R^+$, $RS^+$, $RRSH^+$, and $(RS)_2$, which are characteristic signatures of the thiol mass spectrum. From the absence of disulfide band in the IR spectra, we attribute the $(RSSH)^+$ and $(RS)_2$ peaks to ion/molecule reactions upon desorption. All the desorptions occur at approximately 550 K, close to the value obtained from thermogravimetric analysis.

Each molecule of MPC has a compact, crystalline metal core. This metallic core of 1–4 nm size is encapsulated within a shell of tightly packed hydrocarbon chains linked to the core via sulfur atoms. Several details of the structure of the core are still unclear, but theoretical and experimental evidence suggests that it is faceted. Electronic and optical properties are structured, showing the effects of conduction-level quantization of a metallic $Au^{(0)}$ or $Ag^{(0)}$ core. XPS, IR, and NMR analyses suggest that it is the thiolate, which is present on the surface. IR studies confirm a fully ordered, crystalline, all-trans arrangement of the long-chain alkanethiols, whereas the short-chain thiols are liquid-like. Absence of S–H stretching in IR indicates that the alkane thiols adsorb on gold/silver by losing the proton. TEM and XRD measurements show that the adjacent Au particles are separated by approximately one chain length, not the expected two chain lengths. This suggests that the long-range ordering arises from the interdigitation of chain domains on neighboring particles.

Stability of the monolayers on the cluster surface is an important issue to be taken care of in their preparation and storage. Studies suggest that these monolayer-protected clusters are stable in air at room temperature for 6 months. Recently, we have shown that ozone can oxidize the monolayer [71], as in the case of 2D SAMs [72]. Sulfur head-group gets oxidized, and this results in desorption of some of the molecules as evidenced by the loss of intensity of the CH modes in the IR spectrum. This results in the aggregation of the clusters. We have also shown the radical-induced core destruction and desorption of the monolayer [73]. This occurs in presence of UV light and chlorinated solvents; the monolayer desorbs from the surface in the form of partially halogenated disulfides. The metal is leached out as chlorides.

## PHASE TRANSITIONS

MD simulations suggest that the monolayers undergo a phase transition near the bulk melting temperature of the alkane residue of the corresponding alkyl thiolate, accompanied by intramolecular conformational changes [66]. A first-order phase transition for both short- and long-chain monolayers is predicted, with the melting temperatures close to that of the corresponding alkyl chain melting values; while the experimental observations of SAMs on planar surfaces suggest that long-chain alkyl thiols melt around 333 K. The melting transition results in changes in the intermolecular structure, that is, from the bundled state to a disordered state. The melting temperature depends on the chain length of the passivating thiol, as well as the cluster core size. It has been shown that the outer boundary chains start to develop gauche defects at lower temperatures than the chains near to the core. At high temperatures, these defects progress toward interior, and after the melting point both the outer and interior chains look the same [74].

Phase transitions in alkanethiolate monolayers on gold clusters have been detected by DSC [75], variable-temperature NMR, and variable-temperature IR spectroscopies [76]. All the clusters with chain lengths more than 8 show a broad endotherm in DSC at 330 K, which indicates a phase transition. This transition is attributed to melting of the alkyl chains. In clusters, because of the high curvature of the surface, the chain termini of the alkyl groups are more diverged than the head-group. This makes the interpenetration of the adjacent alkyl chain termini to this gap, and the van der Waals forces make this structure more ordered and stable. The observed transition was attributed to the melting of the alkyl chains in the interdigitated regions. Enthalpy associated with the transition increases with increasing chain length because larger chain length affords more extensive van der Waals interactions and resulting enthalpic contributions. Badia et al. used variously deuterated octadecanethiolate monolayers for understanding the nature of the phase transition [76]. DSC gives broad endotherms for all samples, suggesting thermally induced reversible phase transitions. They also studied the infrared spectra of these systems as a function of temperature. The results suggest that chain melting begins at the chain terminus and propagates toward the center of the chain as the temperature increases. This result has been confirmed by $^2H$ NMR studies as well [77].

When the alkyl thiols contain terminal groups such as hydroxyl or carboxyl, the transition temperature is found to be higher than that of the methyl-terminated one. This is due to the formation of

hydrogen bonding, which gives higher order and thermal stability. Schmitt et al. carried out a comprehensive study of the phase transition of carboxyl-terminated, alkanethiol-protected gold clusters [78]. They found that at room temperature, these alkyl thiols are all-trans and are in a thermally stable, motionally restricted state with chain melting observed only above 413 K. This is in contrast to the behavior of methyl- or hydroxyl-terminated thiols, where a chain length-dependent transition is observed at a lower temperature [77].

IR studies show that the monolayers undergo a transition from an ordered state to a disordered state at the phase-transition temperature [76]. The methylene stretching modes were shifted from solid- to liquid-like values at higher temperatures. We measured variable temperature IR of the alkanethiol-protected Au and Ag clusters [57]. The $d^+$ and $d^-$ modes show a blue shift with increase in temperature. This suggests the melting of the alkyl chain. This transition seems to be reversible up to 473 K, which is confirmed by the DSC. The transition is reversible, and upon repeating the heating-cooling cycle, the enthalpy of this transition is increased for both Au and Ag clusters. This is attributed to the annealing of the monolayer on the surface.

Neutron scattering is a powerful technique [79] to study the dynamics in condensed matter. Random motion of the particles in the system leads to Doppler broadening of the scattered neutrons,

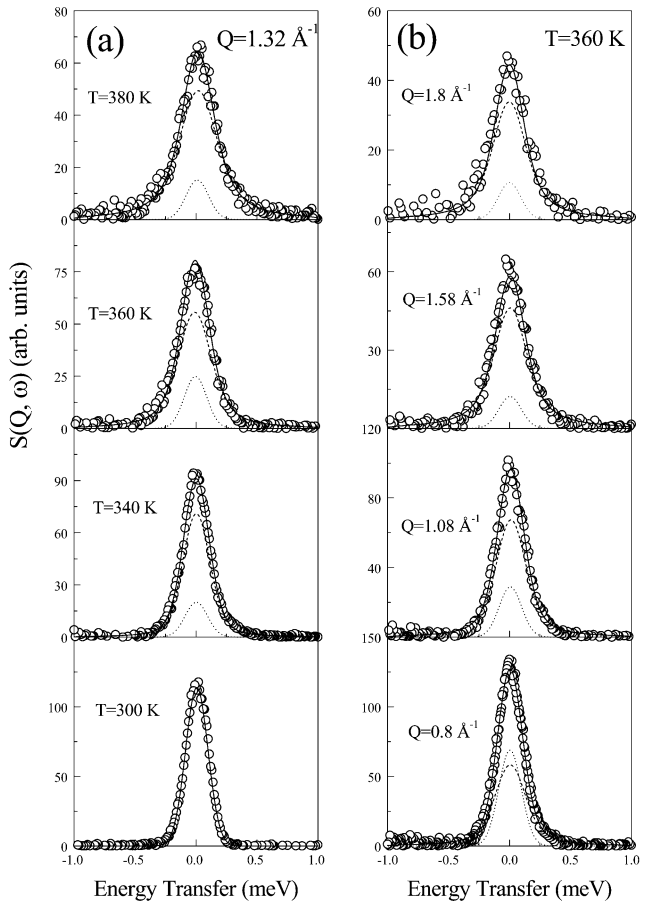


**Fig. 4** Typical QENS spectra for octadecanethiol-protected gold cluster (a) at $Q$ = 1.32 Å$^{-1}$ and at different temperatures (b) at 360 K, but at different $Q$ values. Dashed and the dotted lines are the quasielastic and elastic components, respectively (from Mitra et al. [80], copyright American Chemical Society).

which results in the broadening of the elastic line known as quasielastic neutron scattering (QENS). The QENS not only provides the time scale but also the geometry of motions. Recently, we monitored the alkyl chain dynamics in monolayer-protected clusters by neutron scattering [80]. Figure 4 shows the QENS spectra for octadecanethiol-protected gold cluster at different Q values and at different temperatures. It is seen that the alkyl chains are rotationally frozen in Au clusters, and dynamics evolve slowly. In the cluster superlattices of silver, however, noninterdigitated chains show dynamics at room temperature, and beyond chain-melting temperature, all alkyl chains contribute to dynamics. Activation energy of rotation is found to be 6.3 ± 0.4 kcal/mol. The model suggests that the alkyl chains are close-packed with a nearest neighbor distance of 4.2 Å, implying that the chains are stretched and extended on the cluster surface.

## SUMMARY

SAMs on Au(111) and Ag(111) present ($\sqrt{3} \times \sqrt{3}$) R30° and ($\sqrt{7} \times \sqrt{7}$) R10.9° overlayers, respectively; the structures are a balance between the energetics of S-metal chemisorption and interchain interaction. The structure of organic thiol and dithiol monolayers differ significantly from that of alkane thiols. Various experiments suggest that alkanethiol SAMs on planar surfaces are more ordered at very low temperature (~200 K). As temperature increases, alkyl chains undergo a transition from an ordered phase to another ordered phase at around 300 K. At this temperature, gauche defects are concentrated at the chain termini. Further increase in temperature to 318 K causes untilting of the alkyl chain. A rotator phase also has been observed at this temperature. Thermal motion of the alkyl chain causes the movement of the top-most layer of surface gold atoms. This results in the formation of vacancy island and an ordered SAM at a reduced coverage. At still higher temperatures (~350 K), the gauche conformations diffuse through the middle of the chains because of the availability of free volume due to chain untilting. The alkyl chains behave like a liquid at this temperature. These experiments prove that SAMs undergo an orientational and conformational change upon heating. The transition temperature varies with the chain length of the thiol.

Metal nanoparticles are highly faceted with (111) and (100) faces, and hence the monolayers on them can be compared with those on planar surfaces. Various studies suggest that there is an excellent correspondence between the chain length-dependent order/disorder phase transitions observed in the two systems. There is a higher alkanethiolate surface density on the nanoparticles (15.4 $Å^2$/molecule) as compared to the flat Au(111) surface (21.4 $Å^2$/molecule). The greater concentration of surface defect sites and the high radius of curvature of the cluster allows a larger proportion of the gold atoms to be on the cluster surface, which in turn results in the greater coverage of the monolayers on the surface. SAMs on nanocrystallites exhibit a greater packing density, where the ratio of the number of exposed gold atoms to the number of exposed sulfur atoms is between 1.55 to 1.87 in smaller and larger crystallites, respectively. The ratio is 3 in SAMs on a planar gold surface. However, the surface density of the monolayers is almost four times greater than that near the terminal $CH_3$ group. This results in the greater mobility of the terminal group, as well as a large tilt angle. Both in 2D and 3D SAMs, alkanethiols assume a fully all-trans zigzag conformation with gauche defects concentrated at the chain termini. The defect concentration increases with increasing temperature and decreases with increasing pressure. Kinetic study on 2D monolayers establishes a two-step mechanism in their formation, whereas such studies do not exist for monolayers on cluster surfaces. Both 2D and 3D SAMs are stable in air, and they undergo oxidation in presence of ozone.

Alkanethiol SAMs on planar and cluster surfaces undergo melting prior to desorption. This temperature is dependent on the chain length of the thiol, the longer one melts at higher temperature. In the case of cluster surface, this depends on the size of the cluster also. Transition temperature is greater than the melting point of the bulk thiol. There is a higher degree of order in the monolayers relative to the bulk materials, which is due to the restriction imposed by the Au–S bond. Studies show that the melting transition is first order. Various studies on 2D SAMs clearly demonstrate the existence of more than

one transition, whereas such information is not available for SAMs on the cluster surface. Only melting transition is observed in the latter. Energetics of transitions of 3D SAMs is well established, whereas not much is known about 2D SAMs.

## ACKNOWLEDGMENTS

The work described here was performed by several graduate students. We thank all our collaborators. Financial support from the Department of Science and Technology and the Council of Scientific and Industrial Research is acknowledged.

## REFERENCES

1. I. Langmuir. *J. Am. Chem. Soc*. **39***,* 1848 *(*1917).
2. K. B. Blodgett. *J. Am. Chem. Soc*. **57**, 1007 (1935).
3. W. C. Bigelow, D. L. Picket, W. P. Zisman. *J. Coll. Inter. Sci.* **1**, 513 (1946).
4. R. G. Nuzzo and D. L. Allara. *J. Am. Chem. Soc.* **105**, 4481 (1983).
5. J. Sagiva and K. Taya. *J. Am. Chem. Soc.* **102**, 92 (1980).
6. H. Ogawa, T. Chihera, K. Taya. *J. Am. Chem. Soc.* **107**, 1365 (1985).
7. A. Ulman. *An Introduction to Ultrathin Organic Films*: *From Langmuir Blodgett to Self-Assembly,* Academic, New York (1991).
8. L. J. Kepley, R. M. Crooks, A. J. Ricco. *Anal. Chem.* **64**, 3191 (1992).
9. Y. Yamamoto, H. Nishihara, K. Aramaki. *J. Electrochem. Soc.* **140**, 436 *(*1993).
10. L. Häussling, B. Michel, H. Ringsdorf, H. Rohrer. *Angew. Chem. Int. Ed. Eng.* **30**, 569 (1991).
11. L. M. Frostman, M. M. Bader, M. D. Ward. *Langmuir* **10**, 576 (1994).
12. D. L. Allara. *Biosens. Bioelectron.* **10**, 771 *(*1995).
13. M. Brust, M. Walker, D. Bethell, D. J. Schiffrin, R. Whyman. *J. Chem. Soc. Chem. Commun.* 801 (1994).
14. A. Ulman. *Chem. Rev.* **96**, 1533 (1996).
15. G. E. Poirier. *Chem. Rev*. **97**, 1117 (1997).
16. F. Schreiber. *Prog. Surf. Sci*. **65**, 151 (2000).
17. M. J. Hostetler and R. W. Murray. *Curr. Opin. Colloid Interface Sci.* **2**, 42 (1997).
18. A. C. Templeton, W. P. Wuelfing, R. W. Murray. *Acc. Chem. Res.* **33**, 27 (2000).
19. S. Eu and W. K. Paik. *Mol. Cryst. Liq. Cryst.* **337**, 49 *(*1999).
20. W. K. Paik, S. Eu, K. Lee, S. Chon, M. Kim. *Langmuir* **16**, 10198 (2000).
21. B. George, T. Utschig, N. Sandhyarani, T. Pradeep. To be submitted.
22. M. Zarinkov, S. Frey, H. Rong, Y.-J. Yang, K. Heister, M. Buck, M. Grunze. *Phys. Chem. Chem. Phys.* **2**, 3359 (2000).
23. P. Fenter, A. Eberhardt, K. S. Liang, P. Eisenberger. *J. Chem. Phys*. **106**, 1600 (1997).
24. G. E. Poirier and M. J. Tarlov. *Langmuir* **10**, 2853 (1994).
25. C. Schonenberger, J. A. M. Sondaghuethorst, J. Jorritsma, L. G. J. Fokkink. *Langmuir* **10***,* 611 (1994*)*.
26. J. P. Bucher, L. Santesson, K. Kern. *Langmuir* **10**, 979 (1994).
27. A. Nemetz, T. Fischer, A. Ulman, W. Knoll. *J. Chem. Phys.* **98**, 5912 (1993).
28. M. Zharnikov and M. Grunze. *J. Phys. Condens. Matter*. **13**, 11333 (2001).
29. K. V. G. K. Murty, M. Venkataramanan, T. Pradeep. *Langmuir* **14**, 5446 (1998).
30. S. W. Joo, S. W. Han, K. Kim. *J. Phys. Chem. B* **103**, 10831 (1999).
31. M. Venkataramanan, K. V. G. K. Murty, T. Pradeep, W. Deepali, K. Vijayamohanan. *Langmuir* **16**, 7673 (2000).
32. N. Sandhyarani and T. Pradeep. *J. Coll. Interface Sci*. **218**, 176 (1999).
33. S. W. Han, and K. Kim. *J. Coll. Interface Sci*. **240**, 492 (2001).

34. T. Nakamura, R. Kimura, F. Matsui, H. Kondoh, T. Ohta, H. Sakai, M. Abe, M. Matsumoto. *Langmuir* **16**, 4213 (2000).
35. K. Bandyopadhyay, K. Vijayamohanan, M. Venkataramanan, T. Pradeep. *Langmuir* **15**, 5314 (1999).
36. M. Venkataramanan, G. Skanth, K. Bandhyopadhyay, K. Vijayamohanan, T. Pradeep. *J. Coll. Interface. Sci*. **212**, 553 (1999).
37. N. Sandhyarani, S. Berchmans, V. Yegnaraman, T. Pradeep. *J. Coll. Interface Sci.* **209**, 154 (1999).
38. T. Pradeep, C. Evans, J. Shen, R. G. Cooks. *J. Phys. Chem. B* **103**, 5304 (1999).
39. T. Pradeep, J. Shen, C. Evans, R. G. Cooks. *Anal. Chem.* **71**, 3311 (1999).
40. M. A. Bryant and J. E. Pemberton. *J. Am. Chem. Soc.* **113**, 8284 (1991).
41. M. A. Bryant and J. E. Pemberton. *J. Am. Chem. Soc*. **113**, 3629 (1991).
42. N. Sandhyarani and T. Pradeep. *Vacuum* **49**, 279 (1998).
43. V. Bindu and T. Pradeep. *Vacuum* **49**, 63 (1998).
44. C. E. D. Chidsey, G.-Y. Liu, P. Rowntree, G. Scoles. *J. Chem. Phys.* **94**, 8493 (1991).
45. N. Camillone III, C. E. D. Chidsey, G.-Y. Liu, T. M. Putvinski, G. Scoles. *J. Chem. Phys.* **94**, 8493 (1991).
46. R. G. Nuzzo, E. M. Korenic, L. H. Dubois. *J. Chem. Phys.* **93**, 767 (1990).
47. J. Hautman and M. Klein. *J. Chem. Phys.* **93**, 7483 (1990).
48. W. Mar and M. L. Klein. *Langmuir* **10**, 188 (1994).
49. J. Hautman and M. Klein. *J. Chem. Phys.* **91**, 4994 (1989).
50. C. Taut, A. J. Pertsin, M. Grunze. *Langmuir* **12**, 3481 (1996).
51. R. Bhatia and B. J. Garrison. *Langmuir* **13**, 765 (1997).
52. A. F. Sadreev and Y. V. Sukhinin. *J. Chem. Phys.* **107**, 2643 (1997).
53. L. H. Dubois, B. R. Zegarik, R. G. Nuzzo. *J. Electro. Spect. Relat. Phen.* **54/55**, 1143 (1990).
54. F. Bensebaa, T. H. Ellis, A. Badia, R. B. Lenox. *J. Vac. Sci. Tech. A* **13**, 1331 (1995).
55. F. Bensebaa, T. H. Ellis, A. Badia, R. B. Lenox. *Langmuir* **14**, 2361 (1998).
56. F. Bensebaa, T. H. Ellis, E. Kruus, R. Voicu, Y. Zhou. *Langmuir* **14**, 6579 (1998).
57. N. Sandhyarani, M. P. Antony, G. Panneer Selvam, T. Pradeep. *J. Chem. Phys.* **113**, 9794 (2000).
58. R. Voicu, A. Badia, F. Mrin, R. B. Lennox, T. H. Ellis. *Chem. Mater*. **13**, 2266 (2001).
59. P. Fenter, P. O. Eisenberger, K. S. Liang. *Phys. Rev. Lett.* **70**, 2447 (1993).
60. A. Badia, R. Back, R. B. Lenox. *Angew. Chem., Int. Ed. Engl.* **33**, 2332 (1994).
61. J.-P. Bucher, L. Santesson, K. Kern. *Langmuir* **10**, 979 (1994).
62. M. Venkataramanan and T. Pradeep. *Anal. Chem.* **72**, 5852 (2000).
63. G. E. Poirier, W. P. Fitts, J. M. White. *Langmuir* **17**, 1176 (2001).
64. G. Schmid. *Chem. Rev.* **92**, 1709 (1992).
65. K. Vijaya Sarathy, G. U. Kulkarni, C. N. R. Rao. *J. Chem. Soc. Chem. Comm.* 537 (1997).
66. W. D. Luedtke and U. Landman. *J. Phys. Chem.* **100**, 13323 (1996).
67. R. H. Terril, T. A. Postlethwaite, C.-H. Chen, C.-D. Poon, A. Terzis, A. Chen, J. E. Hutchison, M. R. Clark, G. Wignall, J. D. Londono, R. Superfine, M. Falvo, C. S. Johnson, E. T. Samulski, Jr., R. W. Murray. *J. Am. Chem. Soc.* **117**, 12537 (1995).
68. M. J. Hostetler, J. J. Stokes, R. W. Murray. *Langmuir* **12**, 3604 (1996).
69. A. Badia, L. Denners, L. Dickinson, F. G. Morin, R. B. Lennox, L. Reven. *J. Am. Chem. Soc.* **119**, 11104 (1997).
70. N. Sandhyarani, M. R. Resmi, R. Unnikrishnan, K. Vidyasagar, Shuguang Ma, M. P. Antony, G. P. Selvam, V. Visalakshi, N. Chandrakumar, K. Pandian, Y.-T. Tao, T. Pradeep. *Chem. Mater.* **12**, 104 (2000).
71. N. Sandhyarani and T. Pradeep. *Chem. Phys. Lett.* **338**, 33 (2001).
72. M. H. Schoenfisch and J. E. Pemberton. *J. Am. Chem. Soc*. **120**, 4502 (1998).
73. N. Sandhyarani, T. Pradeep, J. Fransisco. *Chem. Phys. Lett.* **342**, 272 (2001).

74. W. D. Luedtke and U. Landman. *J. Phys. Chem. B* **102**, 6566 (1998).
75. A. Badia, S. Singh, L. Demers, L. Cuccia, G. R. Brown, R. B. Lennox. *Chem. Eur. J.* **2**, 359 (1996).
76. A. Badia, L. Cuccia, L. Demers, F. Morin, R. B. Lennox. *J. Am. Chem. Soc*. **119**, 2682 (1997).
77. A. Badia, W. Gao, S. Singh, L. Demers, L. Cuccia, L. Reven. *Langmuir* **12**, 1262 (1996).
78. H. Schmitt, A. Badia, L. Dickinson, R. B. Lennox. *Adv. Mater*. **10**, 475 (1998).
79. M. Bee. *Quasielastic Neutron Scattering*, Adam-Hilger, Bristol (1988).
80. S. Mitra, B. Nair, T. Pradeep, P. S. Goyal, R. Mukhopadhyay. *J. Phys. Chem. B* **106**, 3960 (2002).